Symmetry and Neuroscience

Martin Golubitsky[1]

1 Introduction

We discuss the question: Is symmetry a useful tool in neuroscience? Even though symmetry has been important in many aspects of physics and engineering, it may appear to be an unlikely part of the structure of the nervous system. However, there are at least three rather different areas of neuroscience where symmetry does have a role to play: animal gaits, the visual cortex, and the vestibular system; and this talk will describe how symmetries enter into the these areas. My point of view is the one discussed in *The Symmetry Perspective* [17].

As an overview Schöner, Jiang, and Kelso [32] and Collins and Stewart [10] point out that standard quadrupedal gaits (walk, trot, pace, etc.) are highly stylized symmetric motions. Collins and Stewart observe that these symmetries suggest a structure for locomotor central pattern generators (CPG), where a CPG is a collection of neurons that produce the rhythms associated to the varous gaits. Moreover, understanding the rhythms associated to these gaits leads to interesting mathematics concerning the spatiotemporal symmetries of periodic solutions of ODEs.

Ermentrout, Cowan, and Bressloff [12, 5, 6] exploit symmetries in the connectivity of the primary visual cortex (electrical signals are sent from the retina to the lateral geniculate nucleus and then to the primary visual cortex) to create models for this system, and use the symmetries to explain the form that geometric visual hallucinations take. Finally, McCollum and Boyle [29] show that the neuroconnectivity between the semicircular canals in the inner ear and the ring of muscles surrounding the neck has octahedral symmetry.

In each of these examples, the symmetry group needs to be identified either through the symmetries found in system outputs (gaits, hallucinations) or in the actual neurobiology (primary visual cortex, vestibular system). In addition, in order to be useful in modeling, the spaces on which these symmetries act must be identified — and usually these spaces are understood using the phase spaces of coupled systems of ODEs [35, 23]. For example, the simplest models for quadrupedal gaits are based on the group $\mathbf{Z}_4 \times \mathbf{Z}_2$ acting on $\mathbf{R}^8$ (its right regular representation); the simplest model for orientation sensitivity in the visual cortex is given by the planar Euclidean group $\mathbf{E}(2)$ acting on itself by group multiplication; and the simplest model of the canal-neck projection of the vestibular system appears to be the octahedral group (rotational symmetries of the cube) acting on $\mathbf{R}^7$.

How important are these symmetries? That remains to be determined. But, at the very least, these are curious and interesting observations. We discuss each in turn. The presentation on gaits follows [18, 17]; the presentation on the visual cortex follows [5, 16]; and the presentation on the vestibular system follows [22].

[1]Department of Mathematics, University of Houston, Houston TX 77204-3008. E-mail: mg@uh.edu

2 Animal Locomotion

We discuss how the spatiotemporal symmetries of the standard quadrupedal gaits of walk, trot, and pace lead to a minimal symmetric network of ODEs that can produce periodic solutions with the same symmetries as these gaits; and how this network then suggests the existence of a rather surprising gait.

Indeed, the general phenomenology of symmetric networks can be illustrated in the context of animal locomotion [7, 9, 10, 19, 20]. It has long been recognized that legged locomotion involves a variety of standard spatio-temporal patterns, in which the legs move periodically in a particular sequence and with particular phase relationships. The case of quadrupeds is especially familiar. For example, when a horse trots, diagonally opposed legs are synchronized, but the two diagonals are half a period out of phase. When the horse walks, the legs hit the ground in the sequence left rear, left front, right rear, right front (or its left/right mirror image) at intervals of one quarter period. When a camel or giraffe paces, its left legs are synchronous, its right legs are synchronous, but left and right are half a period out of phase. More complex gaits, such as the gallop, have phase shifts that are not such simple fractions of the period, leading to a distinction between *primary* gaits with very rigid, simple phase shifts, and *secondary* gaits with more arbitrary and more flexible ones. Figure 1 shows seven common quadruped gaits. Dogs tend to walk, trot, and transverse gallop; squirrels bound; camels tend to pace and rotary gallop; and deer often pronk (all legs moving in synchrony) when startled.

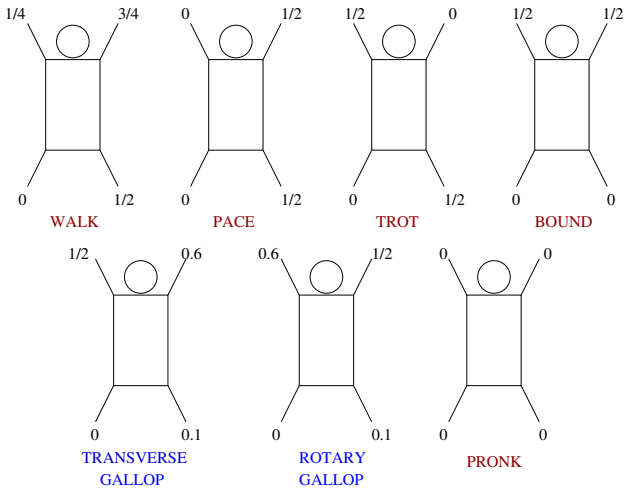

Figure 1: Seven quadrupedal gaits. Numbers indicate the percentage of the time through the gait when the associated leg first strikes the ground. Gaits begin when left hind leg strikes ground.

The symmetry approach to gaits aims to provide a rationale for these patterns, and to explain the distinction between primary and secondary gaits. It tackles these problems by seeking the schematic form of the animal's central pattern generator (CPG), see Kopell and

Ermentrout [28]. The CPG is a network of neurons that is widely believed to generate nerve signals with the corresponding gait spatio-temporal rhythms. Its existence is supported by much indirect evidence, see for example Grillner and Wallén [25], but significant information on the detailed structure of the CPG is known only for a few animals, notably the lamprey, see for example Grillner *et al.* [24]. For most animals even the existence of a CPG has not been confirmed directly, though it is well established that the basic rhythms of locomotion are generated somewhere in the spinal cord, not in the brain. It therefore makes sense to try to infer qualitative information about the CPG from the gaits themselves. Such inferences must start by making some assumptions about the nature of the CPG and how it relates to the gaits, and the consequent deductions are only as good as those assumptions.

We consider three issues: the spatiotemporal symmetries of periodic solutions to systems of ODEs with examples given by quadruped locomotion, the structure that a minimal network of coupled systems of ODEs must have in order to produce periodic solutions with prescribed spatiotemporal symmetries, and a prediction made by this minimal model.

Coupled Cell Networks

For the purpose of this talk a *coupled cell system* is a collection of identical systems of ODE, or *cells*, that are identically coupled. The *network* is a graph whose nodes are the cells and whose arrows indicate which cells are coupled to which. The beginnings of a general theory for the dynamics of coupled cell networks has been developed in [35, 23, 18].

The simplest coupled cell network is the two-cell one in Figure 2. We associate with this network a class of differential equations, which we call *admissible*. For this network the admissible differential equations are those of the form

$$\begin{aligned} \dot{x}_1 &= g(x_1, x_2) \\ \dot{x}_2 &= g(x_2, x_1) \end{aligned} \tag{2.1}$$

where $x_1, x_2 \in \mathbf{R}^k$ are the state variables of the individual cells. Observe that a single function $g : \mathbf{R}^k \times \mathbf{R}^k \to \mathbf{R}^k$ defines the system.

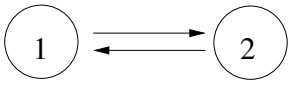

Figure 2: Schematic of a two identical cell identical coupling network.

One consequence of the $\mathbf{Z}_2$ symmetry of this system is the existence of solutions in which $x_1(t) = x_2(t)$ for all t. This follows because the diagonal subspace $\{x : x_1 = x_2\}$ is invariant under the flow of the differential equation for all g. For all such solutions, the two cells behave synchronously. In particular, there is a nonempty open set of functions g for which these systems have synchronous periodic solutions.

Another consequence of symmetry is that there exists a non-empty open set of functions g for which there is a periodic solution, with period T, such that $x_2(t) = x_1(t + T/2)$ for all t, see [21, 17]. That is, the two cells have the same periodic dynamics except for a

relative phase shift of half a period. The existence of these two types of periodic solutions generalizes to the class of admissible vector fields for symmetric networks as follows.

Spatiotemporal Symmetries of Periodic Solutions

A symmetry of an ordinary differential equation (ODE) is a transformation that sends solutions to solutions. More specifically, let $\gamma : \mathbf{R}^n \to \mathbf{R}^n$ be a linear map. A system of differential equations

$$\dot{x} = f(x) \tag{2.2}$$

(where $x \in \mathbf{R}^n$ and $f : \mathbf{R}^n \to \mathbf{R}^n$ is smooth) has *symmetry* γ if $\gamma x(t)$ is a solution to (2.2) whenever $x(t)$ is a solution. It is straightforward to verify that γ is a symmetry if and only if f satisfies the *equivariance condition*

$$f(\gamma x) = \gamma f(x) \tag{2.3}$$

Suppose that the system (2.2) has a finite symmetry group Γ. We first note that symmetry forces the existence of many flow invariant subspaces. Suppose that $\Sigma \subset \Gamma$ is a subgroup. Then

$$\mathrm{Fix}(\Sigma) = \{x \in \mathbf{R}^n : \sigma x = x \ \ \forall \sigma \in \Sigma\}$$

is a flow-invariant subspace. (Proof: $\sigma f(x) = f(\sigma x) = f(x)$ for each $x \in \mathrm{Fix}(\Sigma)$. Hence $f : \mathrm{Fix}(\Sigma) \to \mathrm{Fix}(\Sigma)$.) In case Γ is the symmetry group of a network (that is, Γ is a permutation group of the cells), the fixed-point subspaces are generalized diagonals and flow-invariance implies synchrony.

Second, phase-locking is also a natural consequence of symmetry. Suppose that $x(t)$ is a T-periodic solution to (2.2) and that γ is a symmetry. Then either $\gamma x(t)$ is a different periodic trajectory from $x(t)$, or it is the same trajectory. In the latter case, the only difference is a time-translation. That is, $\gamma x(0) = x(\theta)$ for some θ, and uniqueness of solutions implies that $\gamma x(t) = x(t + \theta)$ for all t. Define

$$\begin{array}{rcll} H & = & \{\gamma \in \Gamma : \gamma\{x(t)\} = \{x(t)\}\} & \text{spatiotemporal symmetries} \\ K & = & \{\gamma \in \Gamma : \gamma x(t) = x(t) \quad \forall t\} & \text{spatial symmetries} \end{array}$$

Note that since fixed-point subspaces are flow-invariant, K is an isotropy subgroup of the action of Γ on $\mathbf{R}^n$. In addition, for each $h \in H$, there is a phase shift $\theta(h) \in \mathbf{S}^1$ such that $hx(t) = x(t + \theta(h))$. Moreover, $\theta : H \to \mathbf{S}^1$ is a group homomorphism with kernel K. It follows that H/K is isomorphic to a finite subgroup of $\mathbf{S}^1$ and hence is cyclic.

Periodic solutions with spatiotemporal symmetries are classified as follows.

Theorem 2.1 (H/K Theorem [7, 17]) *Let Γ be a prmutation group which is the symmetry group of a coupled cell network in which all cells are coupled and the internal dynamics of each cell is at least two-dimensional. Let $K \subset H \subset \Gamma$ be a pair of subgroups. Then there exist periodic solutions to some coupled cell system with spatiotemporal symmetries H and spatial symmetries K if and only if H/K is cyclic and K is an isotropy subgroup.*

Four Cells Do Not Suffice

The simplest model of a quadruped locomotor CPG has four identical cells, where it is presumed that the output signal from each cell is sent to one leg. See Figure 3. We ask whether it is possible to couple these four cells in such a way that network systems can naturally produce rhythms associated with the three gaits walk, trot, and pace, and show that it is not [7].

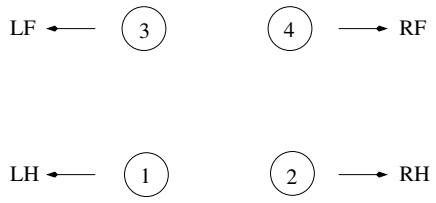

Figure 3: Signal from cell 1 is sent to left hind (LH) leg, etc.

To justify this negative statement we discuss three points:

(a) Gaits rhythms are described by spatiotemporal symmetries.

(b) The symmetry groups of trot and pace cannot be conjugate.

(c) The symmetry group of trot and pace are always conjugate in any four-cell network that also produces a walk.

(a) Collins and Stewart [10] observed that standard quadruped gaits are distinguished by spatiotemporal symmetries, where the space symmetries are leg permutations. The generators for the symmetry groups of trot, pace, and walk are listed in Table 1. In our models we assume that gait rhythms are exact and robust. We also assume that the only robust phase shifts of periodic solutions that are given in these models are those that are described by symmetry.

Gait	Generators of spatio-temporal symmetries			Solution form
Trot	$((1\ 2)(3\ 4), \frac{1}{2})$	and	$((1\ 3)(2\ 4), \frac{1}{2})$	$(x(t), x(t+\frac{1}{2}), x(t+\frac{1}{2}), x(t))$
Pace	$((1\ 2)(3\ 4), \frac{1}{2})$	and	$((1\ 3)(2\ 4), 0)$	$(x(t), x(t+\frac{1}{2}), x(t), x(t+\frac{1}{2}))$
Walk	$((1\ 3\ 2\ 4), \frac{1}{4})$			$(x(t), x(t+\frac{1}{2}), x(t+\frac{1}{4}), x(t+\frac{3}{4}))$

Table 1: Legs are numbered by the associated cells in Figure 3. The permutation (1 2)(3 4) swaps left and right legs; the permutation (1 3)(2 4) swaps front and back legs; fractions indicate phase shift as a fraction of a gait period.

(b) Experiments on dogs imply that trot and pace are not gaits that can be modeled by conjugate solutions. Note that in a system of differential equations conjugate solutions differ only by initial conditions and have the same stability. Blaszczyk and Dobrzecka [2]

indicate that the stability of pace and trot are not the same. In their experiment, a dog's legs are restrained so that they can use a pace at intermediate speeds, but not a trot, which is the dog's preferred gait. Different dogs are placed in this device for two to six months. In post-restraint trials dogs that were in the shorter restraint period switched back to a trot quickly with only occasional use of a pace. Occurrence of the pace was more frequent in the animals that were restrained for a longer period, but the use of pace decreased with every post-restraint experimental trial.

(c) It follows from (a) that if a four-cell network is coupled so that periodic solutions with the rhythm of a walk occur naturally, then the permutation (1 3 2 4) must be a network symmetry. Suppose that the system also produces a pace solution. As indicated in Figure 4, cells 1 and 3 and cells 2 and 4 must be synchronous. As illustrated in that figure, applying the walk symmetry to that solution produces a solution in which cells 1 and 4 and cells 2 and 3 are synchronous — a pace. It follows that trot and pace solutions are conjugate in any four-cell network that can produce a robust walk.

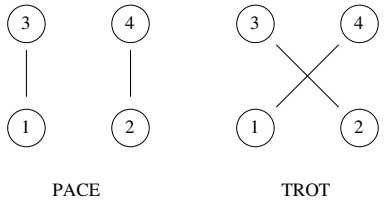

Figure 4: Lines between cells indicate synchrony; no lines indicate half-period phase shifts.

The Eight-Cell Network

Golubitsky *et al.* [7, 20] make six assumptions, and deduce that for quadrupeds the only possible symmetry class of CPG networks is the 8-cell network shown in Figure 5. The details of the deduction are unimportant here, but they are explicit in the original paper.

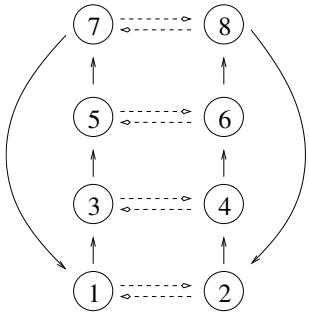

Figure 5: Eight-cell network for quadrupeds. Dashed lines indicate contralateral coupling; single lines indicate ipsilateral coupling.

This network has eight symmetries—permutations of the legs (more precisely, the leg

		walk	jump	trot	pace	bound	pronk
LF	RF	$\frac{3}{4}$ $\frac{1}{4}$	$\frac{1}{2}$ $\frac{1}{2}$	$\frac{1}{2}$ 0	0 $\frac{1}{2}$	$\frac{1}{2}$ $\frac{1}{2}$	0 0
LH	RH	$\frac{1}{2}$ 0	$\frac{3}{4}$ $\frac{3}{4}$	0 $\frac{1}{2}$	0 $\frac{1}{2}$	0 0	0 0
LF	RF	$\frac{1}{4}$ $\frac{3}{4}$	0 0	$\frac{1}{2}$ 0	0 $\frac{1}{2}$	$\frac{1}{2}$ $\frac{1}{2}$	0 0
LH	RH	0 $\frac{1}{2}$	$\frac{1}{4}$ $\frac{1}{4}$	0 $\frac{1}{2}$	0 $\frac{1}{2}$	0 0	0 0
Subgroup K		$\mathbf{Z}_2(\kappa\omega^2)$	$\mathbf{Z}_2(\kappa)$	$\mathbf{Z}_4(\kappa\omega)$	$\mathbf{Z}_4(\omega)$	$\mathbf{D}_2(\kappa,\omega^2)$	$\mathbf{Z}_2 \times \mathbf{Z}_4$

Table 2: Phase shifts for primary gaits in the eight-cell network.

labels) that preserve the edges. There are two types of symmetry: contralateral symmetry κ, which interchanges cells on the left with cells on the right, and ipsilateral symmetry ω, which cyclically and simultaneously permutes cells on both left and right. Thus the symmetry group of the eight-cell quadruped CPG is $\Gamma = \mathbf{Z}_2\langle\kappa\rangle \times \mathbf{Z}_4\langle\omega\rangle$.

The H/K Theorem provides a classification of the possible spatio-temporal symmetries. Primary states are characterized by all eight cells having the same waveform modulo phase shift (that is, $H = \Gamma$) whereas secondary gaits involve more than one waveform (that is, $H \subsetneq \Gamma$). It is straightforward to calculate the six subgroups $K \subset H$ for which H/K is cyclic and determine the primary patterns for the 8-cell network: see Table 2. There is an analogous (but more complicated) classification of secondary gaits.

The fact that $H = \Gamma$ implies that the signals $x_i(t)$ and $x_j(t)$ must be the same up to a well defined phase shift. For example, suppose that K is generated by κ and ω^2. Since κ is a K symmetry the outputs from κ related cells must be identical; that is, $x_1(t) = x_2(t)$, etc. Since ω^2 is a K symmetry, $x_1(t) = x_5(t)$, etc. Since ω is an H symmetry that is not in K, it corresponds to a half period phase shift and $x_1(t) = x_3(t + \frac{1}{2})$. For such a periodic solution this model CPG sends synchronous signals to the hind legs, synchronous signals to the fore legs, and the two sets of signals are a half period out of phase. This rhythm corresponds to a bound. The other identifications with gait rhythms are found similarly.

A Prediction: The Jump

The patterns listed in the table correspond to standard primary quadruped gaits, with one exception: the gait we have labelled 'jump'. After performing the above analysis, the jump gait was observed at the Houston Livestock Show and Rodeo. Figure 6 shows four video frames of a bucking bronco, taken at equal intervals of time. The interval between the footfalls is very close to 1/4 of the period of this rhythmic motion.

Indeed, approximately 200 frames of the rodeo video are coded in Figure 7. Dark regions begin when the right hind leg is firmly on the ground and light regions begin when the right fore leg is firmly on the ground. This figure indicates that the average time elapsed from right hind to right fore leg ground strikes is approximately three times the average time elapsed from right fore to right hind leg ground strikes. The *primitive ricocheting jump* of a Norway rat and an Asia Minor gerbil also has the same pattern of phases as the jump

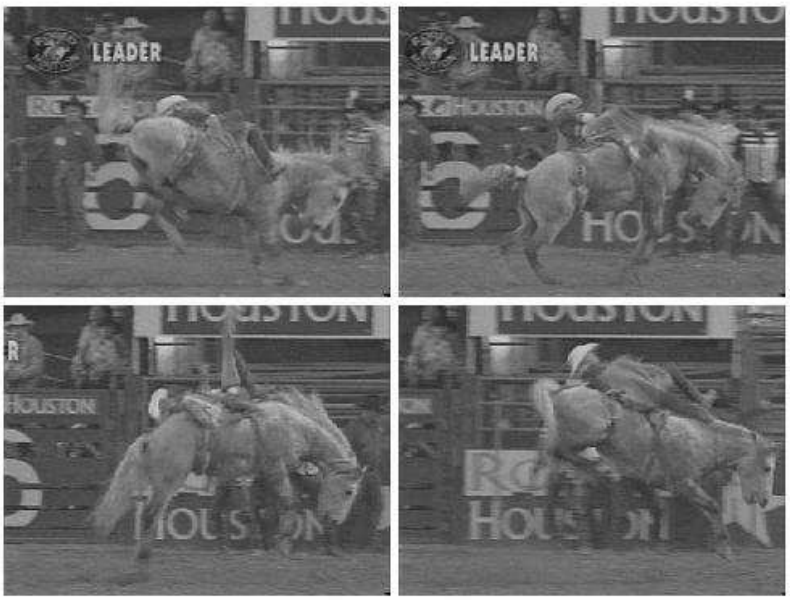

Figure 6: Quarter cycles of bareback bronc jump at Houston Livestock Show and Rodeo. (UL) fore legs hit ground; (UR) hind legs hit ground; (LL) and (LR) all legs in air.

gait, Gambaryan [14].

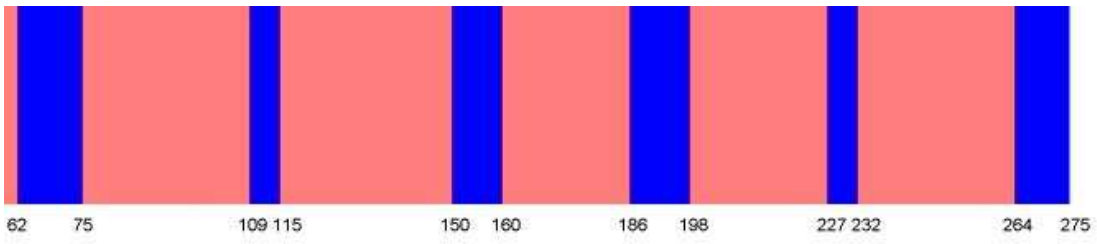

Figure 7: Average right hind to right fore = 31.2 frames (light region); average right fore to right hind = 11.4 frames (dark region); $\frac{31.2}{11.4} = 2.74$.

3 The Primary Visual Cortex

The orientation sensitivity of neurons in the primary visual cortex appears to encode the Euclidean group, acting on itself by group multiplication, as a group of symmetries of the cortex, and these symmetries appear to characterize the kinds of geometric patterns described by individuals undergoing drug-induced visual hallucinations. In earlier work, Bard

Ermentrout and Jack Cowan [12] explained the geometric forms of hallucinations by applying equivariant bifurcation theory to continuum models of the visual cortex. In later work Cowan, along with Paul Bressloff, Peter Thomas, and Matt Wiener [5, 6], proposed using the orientation sensitivity of neurons in the primary visual cortex to refine the symmetry arguments and to obtain results that better coordinated the mathematically generated patterns with the drug induced images. We survey how symmetry appears in the cortex and how it is used to construct the hallucinatory patterns.

A Short Review of Geometric Hallucinations

In the 1930's Klüver classified geometric visual hallucinations into four groups of *form constants* (see [27, p. 66]): honeycombs, cobwebs, tunnels, and spirals. Klüver states on p. 71 "We wish to stress merely one point, namely, that under diverse conditions the visual system responds in terms of a limited number of form constants." Examples of the four form constants are given in Figure 8.

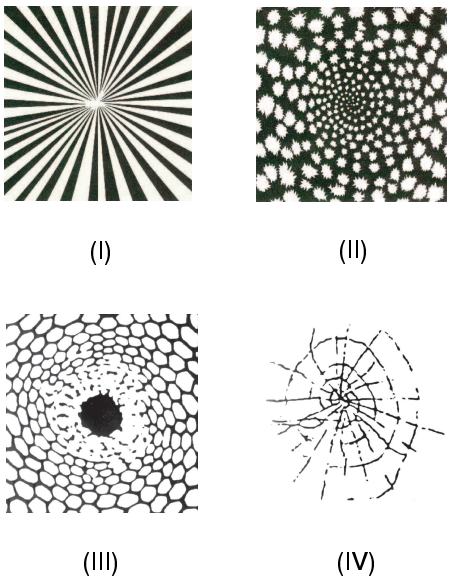

Figure 8: Hallucinatory form constants from [6]. (I) funnel and (II) spiral images seen following ingestion of LSD [redrawn from [33], (III) honeycomb generated by marihuana [redrawn from [8]], (IV) cobweb petroglyph [Redrawn from [30]].

In their mathematical study of drug induced hallucinations Ermentrout and Cowan [12] assumed that the drug uniformly stimulates an inactive cortex and produces, by spontaneous symmetry-breaking, a patterned activity state. The mind then interprets the pattern as a visual image — namely the visual image that would produce the same pattern of activity on the primary visual cortex V1. The Ermentrout-Cowan analysis assumes that a differential equation governs the symmetry-breaking transition from an inactive to an

active cortex and then studies abstractly the transition using standard pattern formation arguments developed for reaction-diffusion and fluid mechanical equations [21, 17]. Their cortical patterns are obtained by thresholding (points where the solution is greater than some threshold are colored black, whereas all other points are colored white). These cortical patterns are then transformed to retinal patterns using the inverse of the retino-cortical map described below (see (3.3)), and these retinal patterns are similar to some of the geometric patterns of visual hallucinations, namely, funnels and spirals.

Orientation Sensitvity of Neurons in the Visual Cortex

It is now well established that neurons in V1 are sensitive to orientations in the visual field. See [26, 15, 1, 3, 5] for more discussion. It is mathematically reasonable to assign an orientation preference to each neuron in V1. Hubel and Wiesel [26] introduced the notion of a *hypercolumn* — a region in V1 containing for each orientation at a single point in the visual field (a mathematical idealization) a neuron sensitive to that orientation.

More recently, Bressloff *et al.* [5] studied the geometric patterns of drug induced hallucinations by including orientation sensitivity. As before, the drug stimulation is assumed to induce spontaneous symmetry-breaking, and the analysis is local in the sense of bifurcation theory. There is one major difference between the approaches in [5] and [12]. Ignoring lateral boundaries Ermentrout and Cowan [12] idealize the cortex as a plane, whereas Bressloff *et al.* [5] take into account the orientation tuning of cortical neurons and idealize the cortex as $\mathbf{R}^2 \times \mathbf{S}^1$. This approach leads to a method for recovering thin line hallucinations such as cobwebs and honeycombs, in addition to the threshold patterns found in the Ermentrout-Cowan theory. See Figure 9.

There are two types of connections between neurons in V1: local and lateral. Experimental evidence suggests that neurons within a hypercolumn are all-to-all connected, whereas neurons in different hypercolumns are connected in a very structured way. This structured lateral coupling is called *anisotropic*, and it is the bifurcation theory associated with anisotropic coupling that is studied in Bressloff *et al.* [5, 4].

The Continuum Models

The Ermentrout and Cowan [12] model of V1 consists of neurons located at each point $\mathbf{x}$ in $\mathbf{R}^2$. Their model equations, variants of the Wilson-Cowan equations [37], are written in terms of a real-valued *activity variable* $a(\mathbf{x})$, where a represents, say, the voltage potential of the neuron at location $\mathbf{x}$.

Bressloff *et al.* [5] incorporate the Hubel-Weisel hypercolumns [26] into their model of V1 by assuming that there is a hypercolumn centered at each location $\mathbf{x}$. Here a *hypercolumn* denotes a region of cortex that contains neurons sensitive to orientation ϕ for each direction ϕ. Their models, also adaptations of the Wilson-Cowan equations [37], are written in terms of a real-valued *activity variable* $a(\mathbf{x}, \phi)$ where a represents, say, the voltage potential of the neuron tuned to orientation ϕ in the hypercolumn centered at location $\mathbf{x}$. Note that angles ϕ and $\phi + \pi$ give the same orientation; so $a(\mathbf{x}, \phi + \pi) = a(\mathbf{x}, \phi)$.

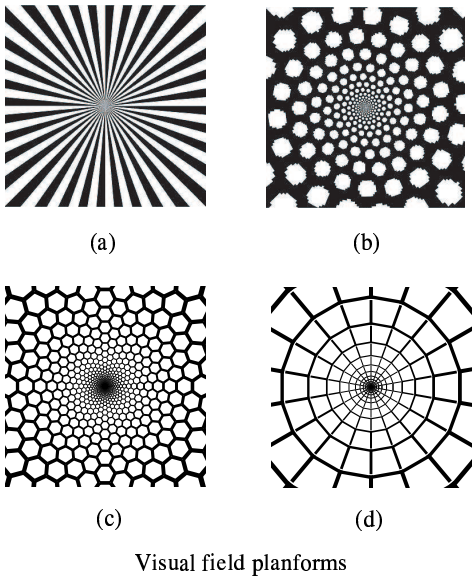

Figure 9: Hallucinatory form constants generated by symmetry-breaking bifurcations on cortex using the shift-twist representation of the Euclidean group, and viewed in retinal coordinates. From [6]. Note the similarities with Figure 8.

The cortical planform associated to $a(\mathbf{x}, \phi)$ is obtained in a way different from the Ermentrout-Cowan approach. For each fixed $\mathbf{x} \in \mathbf{R}^2$, $a(\mathbf{x}, \cdot)$ is a function on the circle. The planform associated to a is obtained through a *winner-take-all* strategy. The neuron that is most active in its hypercolumn is presumed to suppress the activity of other neurons within that hypercolumn. The winner-take-all strategy chooses, for each $\mathbf{x}$, the directions ϕ that maximize $a(\mathbf{x}, \cdot)$, and results in a field of directions. The two approaches to creating planforms can be combined by assigning directions only to those locations $\mathbf{x}$ where the associated maximum of $a(\mathbf{x}, \cdot)$ is larger than a given threshold.

A possible justification for the continuum model that idealizes a hypercolumn at each cortex location is that each location is in fact surrounded by neurons sensitive to all of the possible orientations. This fact suggests that the signal read from the primary visual cortex V1 need not be limited to one orientation from each 'physical' hypercolumn. In V1 there is a grid of physical hypercolumns that is approximately 36×36 in extent. (See [4] and references therein.) It is reasonable to suppose that other layers of the visual cortex receive much more information than a 36×36 matrix of orientation values.

Euclidean Symmetry

The Euclidean group $\mathbf{E}(2)$ is crucial to the analyses in both [12] and [5] — but the way that group acts is different. In Ermentrout-Cowan the Euclidean group acts on the plane by its standard action, whereas in Bressloff *et al.* the Euclidean group acts on $\mathbf{R}^2 \times \mathbf{S}^1$ by

the so-called shift-twist representation, as we now explain.

Bressloff *et al.* [5] argue, based on experiments by Blasdel [1] and Eysel [13], that the lateral connections between neurons in neighboring hypercolumns are *anisotropic*. That anisotropy states that the *strength* of the connections between neurons in two neighboring hypercolumns depends on the orientation tuning of both neurons and on the relative locations of the two hypercolumns. Moreover, this anisotropy is idealized to the one illustrated in Figure 10 where only neurons with the same orientation selectivity are connected and then only neurons that are oriented along the direction of their cells preference are connected. These conclusions are based on work of Gilbert [15] and Bosking *et al.* [3]. In particular, the symmetries of V1 model equations are those that are consistent with the idealized structure shown in Figure 10. Suppose for example that the plane is rotated about the center of the hypercolumn, labeled `hypercolumn` in that figure. Then the connection of that hypercolumn to the rotated hypercolumn in the upper right of Figure 10 will no longer be the direction of their cells orientation preference. This difficulty can be corrected if one simultaneously 'rotates' the circle of orientation preferences in each hypercolumn. See the second identity in (3.1).

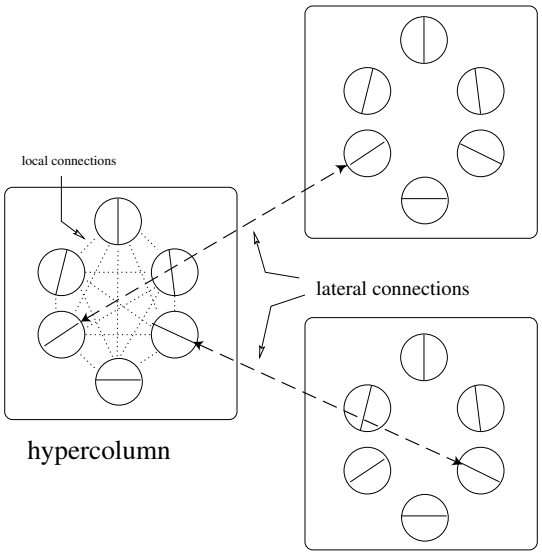

Figure 10: Illustration of isotropic local and anisotropic lateral connection patterns.

The Euclidean group $\mathbf{E}(2)$ is generated by translations, rotations, and a reflection. The action of $\mathbf{E}(2)$ on $\mathbf{R}^2 \times \mathbf{S}^1$ that preserves the structure of lateral connections illustrated in Figure 10 is the *shift-twist* action. This action is given by:

$$\begin{array}{rcl} \mathcal{T}_{\mathbf{y}}(\mathbf{x},\phi) & \equiv & (\mathbf{x}+\mathbf{y},\phi) \\ \mathcal{R}_{\theta}(\mathbf{x},\phi) & \equiv & (R_{\theta}\mathbf{x},\phi+\theta) \\ \mathcal{M}_{\kappa}(\mathbf{x},\phi) & \equiv & (\kappa\mathbf{x},-\phi), \end{array} \tag{3.1}$$

where $(\mathbf{x},\phi) \in \mathbf{R}^2 \times \mathbf{S}^1$, $\mathbf{y} \in \mathbf{R}^2$, κ is the reflection $(x_1,x_2) \mapsto (x_1,-x_2)$, and $R_\theta \in \mathbf{SO}(2)$

is rotation of the plane counterclockwise through angle θ.

Work on optical imaging has made it possible to see how the orientation preference of cells are actually distributed in V1 [1], and a variety of stains and labels have made it possible to see how they are interconnected [13, 3]. Figure 11 shows that the distribution of orientation preferences in the Macaque. In particular, approximately every millimeter there is an *iso-orientation patch* of a given preference.

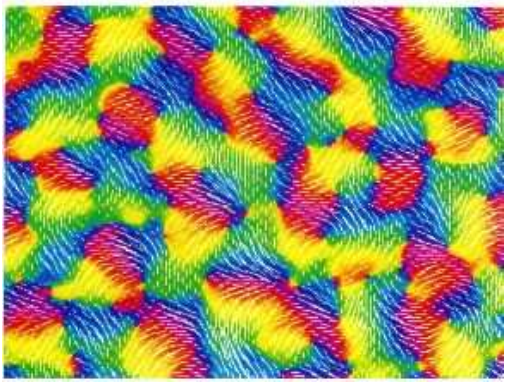

Figure 11: Distribution of orientation preferences in Macaque V1 obtained via optical imaging and using color to indicate iso-orientation patches. Redrawn from [1].

Recent optical imaging experiments combined with anatomical tracer injections suggest that there is a spatial anisotropy in the distribution of patchy horizontal connections, as illustrated in Figure 12. It will be seen from the right panel that the anisotropy is particularly pronounced in the tree shrew. The major axis of the horizontal connections tends to run parallel to the visuotopic axis of the connected cells' common orientation preference. There is also a clear anisotropy in the patchy connections of Macaque, as seen in the left panel.

Symmetry-Breaking Bifurcations on Lattices

Spontaneous symmetry-breaking in the presence of a noncompact group such as the Euclidean group is far from completely understood. One standard approach is to reduce the technical difficulties by looking only for solutions that are spatially doubly periodic with respect to some planar lattice (see [17]); this is the approach taken in [12, 5] and in this study. This approach is justified by the remarkable similarities between the geometric patterns obtained mathematically in [12, 5] and the hallucinatory images reported in the scientific literature [5, 6]. See Figures 8 and 9.

The first step in such an analysis is to choose a lattice type; say a square or hexagonal lattice. The second step is to decide on the size of the lattice. Euclidean symmetry guarantees that at bifurcation, critical eigenfunctions will have *plane wave* factors $e^{2\pi i \mathbf{k}\cdot\mathbf{x}}$ for some critical dual wave vector $\mathbf{k}$. See [4] or [17, Chapter 5]. Typically, the lattice size is chosen

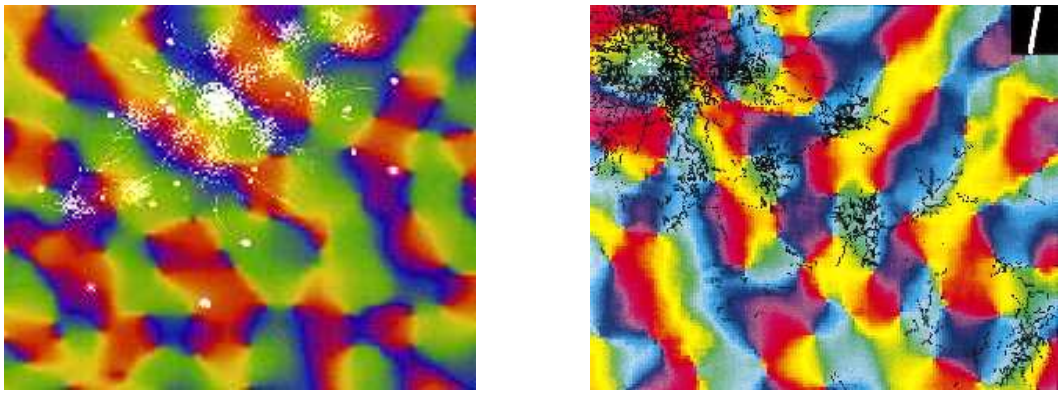

Figure 12: Lateral Connections made by a cells in Macaque (Left panel) and Tree Shrew (Right panel) V1. A radioactive tracer is used to show the locations of all terminating axons from cells in a central injection site, superimposed on an orientation map obtained by optical imaging. Redrawn from [34] and [3].

so that the critical wave vectors will be vectors of shortest length in the dual lattice; that is, the lattice has the smallest possible size that can support doubly periodic solutions.

By restricting the bifurcation problem to a lattice, the group of symmetries is transformed to a compact group. First, translations in $\mathbf{E}(2)$ act modulo the spatial period (which we can take to be 1 on the square lattice) and thus act as a 2-torus $\mathbf{T}^2$. Second, only those rotations and reflections in $\mathbf{E}(2)$ that preserve the lattice (namely, the holohedry $\mathbf{D}_4$ for the square lattice) are symmetries of the lattice restricted problem. Thus, the symmetry group of the square lattice problem is $\Gamma = \mathbf{D}_4 \dot{+} \mathbf{T}^2$. Recall that at bifurcation Γ acts on the kernel of the linearization, and a subgroup of Γ is *axial* if its fixed-point subspace in that kernel is one-dimensional. Solutions are guaranteed by the Equivariant Branching Lemma (see [21, 17]) which states: generically there are branches of equilibria to the nonlinear differential equation for every axial subgroup of Γ. The nonlinear analysis in [4, 12] proceeds in this fashion.

Retinal Images

Finally, we discuss the geometric form of the cortical planforms in the visual field, that is, we try to picture the corresponding visual hallucinations. It is known that the density of neurons in the visual cortex is uniform, whereas the density of neurons in the retina fall offs from the fovea at a rate of $1/r^2$. Schwartz [31] observed that there is a unique conformal map taking a disk with $1/r^2$ density to a rectangle with uniform density, namely, the complex logarithm. This is also called the *retino-cortical* map. It is thought that using the inverse of the retino-cortical map, the complex exponential, to push forward the activity pattern from V1 to the retina is a reasonable way to form the hallucination image — and this is the approach used in Ermentrout and Cowan [12] and in Bressloff *et al.* [5, 6]. Specifically,

the transformation from polar coordinates (r, θ) on the retina to cortical coordinates (x, y) is given in Cowan [11] to be:

$$x = \frac{1}{\varepsilon} \ln\left(\frac{1}{\omega} r\right) \quad \text{and} \quad y = \frac{1}{\varepsilon}\theta \tag{3.2}$$

where ω and ε are constants. See Bressloff *et al.* [6] for a discussion of the values of these constants. The inverse of the retino-cortical map (3.2) is

$$r = \omega \exp(\varepsilon x) \quad \text{and} \quad \theta = \varepsilon y \tag{3.3}$$

In the retinal images, $\omega = 30/e^{2\pi}$ and $\varepsilon = 2\pi/n_h = \pi/18$, where n_h is the number of hypercolumn widths in the cortex, which is taken to be 36.

4 The Vestibular System

In this section we discuss results of McCollum and Boyd [29], as described in Golubitsky, Shiau, and Stewart [22], on the vestibular system, which is a system of tubes with sensors that sense balance and motion. Our purpose is to understand how octahedral symmetry helps to describe the neuronal connections between some of these tubes and the muscle groups in the neck that control head motion.

There are two main components of the vestibular system: the otolith organs, which sense linear acceleration of the head (translation), and the semicircular canals, which sense angular acceleration of the head (rotation). Each ear contains three semicircular canals arranged in three approximately mutually orthogonal planes. See Figure 13.

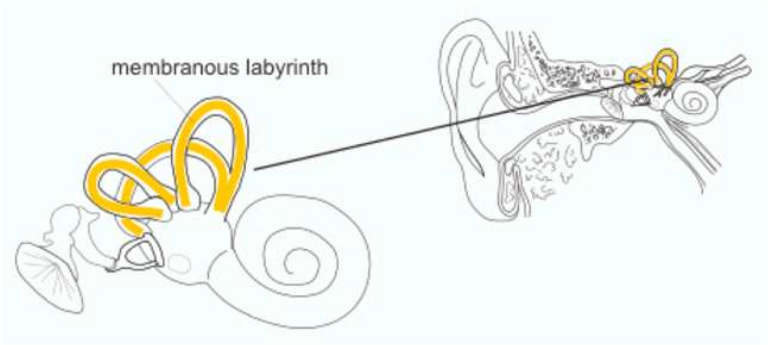

Figure 13: Structure and location of the semicircular canals (right ear). From Vilis [36].

We focus on one aspect of the vestibular system explored by McCollum and Boyd [29]: the network of neurons that conveys signals from the canals to eight principal muscle groups that control the position of the neck, known as the 'canal-neck projection'. The precise structure of the canal-neck projection network appears not to be known, but there is sufficient information to determine its connectivity and hence its symmetries, in an idealized form.

Indeed, McCollum and Boyle [29] show that the canal-neck projection has the symmetries of the octahedral group $\mathbb{O}$ — the symmetry group of a cube. This group consists of 24 rotational symmetries in the usual action by rigid motions in $\mathbf{R}^3$ and of 24 elements that reverse orientation.

We rederive the symmetries in the disynaptic canal-neck projection discussed by McCollum and Boyle [29]. In this aspect of the vestibular system there are six semicircular canals (three in each ear) that are connected to eight muscle groups in the neck.

Polarity Pairs of Canals

The three semicircular canals located in each ear are called *horizontal* h, *anterior* a, and *posterior* p. We denote the six canals by lh, la, lp, rh, ra, rp, where l stands for *left* and r for *right*. Canal hairs are arranged so that fluid flow in one direction in the canal stimulates an excitatory signal and fluid flow in the opposite direction stimulates an inhibitory signal. Moreover, the semicircular canals are paired (lh-rh, la-rp, lp-ra) so that when one member of a pair is transmitting an excitatory signal, then the other member of that pair is transmitting an inhibitory one. These pairs are called *polarity pairs*.

The spatial arrangement of the canals is as follows. There are three (approximately) mutually orthogonal planes. One of these planes is horizontal. The other two are vertical, at an angle of 45° to the plane of left-right symmetry of the head. Each polarity pair consists of two canals that are parallel to one of these planes: one canal in the left ear, one in the right. These two canals are oriented in opposite directions in that plane and detect rotations (actually angular accelerations) of the head about an axis perpendicular to that plane. One member of the polarity pair detects acceleration in one orientation (clockwise or counterclockwise) and the other member detects the opposite orientation.

Connections between Canals and Muscles

Each of the six canals can transmit signals to each of the eight muscle groups. The muscles form four pairs, and if a canal is activated by the motion of the head then it sends an inhibitory signal to one member of each pair and an excitatory signal to the other member. Physiological investigations suggest that each muscle group is excited by a set of three mutually orthogonal canals (that is, one from each polarity pair) and inhibited by the complementary set of canals (the other members of the polarity pairs). We describe the details of this arrangement.

Following McCollum and Boyle, the list of signals transmitted to a given muscle group can be depicted as an 'asterisk', as in Figure 14. Continuous lines represent excitatory signals and dashed lines represent inhibitory signals. Each asterisk has three solid lines (excitatory) and three dotted lines (inhibitory) and diametrically opposite lines have opposite polarity. There are eight possible arrangements of this type. Because the asterisks are drawn in two-dimensional projection, in a conventional orientation with lh between la and lp, there appear to be two kinds of asterisks: two alternating (with excitation and inhibition alternating) and six non-alternating (with three contiguous excitatory canals).

We will shortly see that under a suitable action of the octahedral group, all eight asterisks are equivalent.

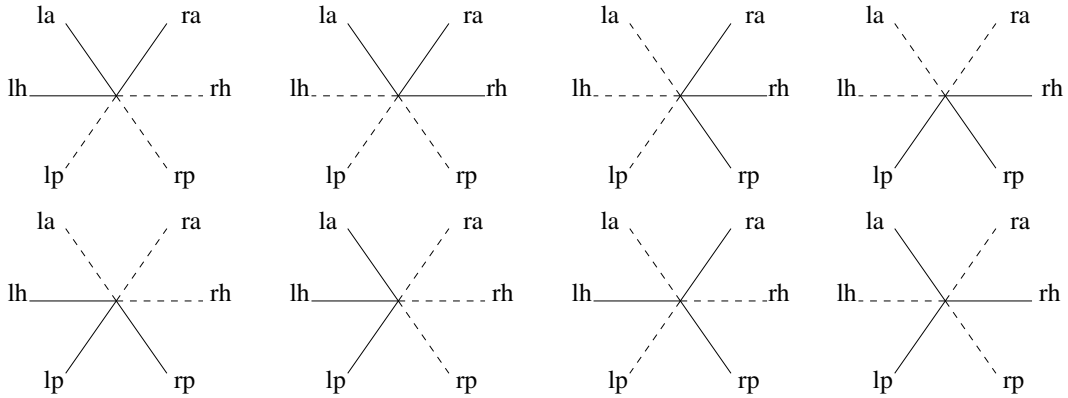

Figure 14: Eight asterisk patterns from six semicircular canals. Continuous lines represent excitatory signals and dashed lines represent inhibitory signals.

The eight neck muscles are shown in Figure 15 and consist of two flexors in the front, two extensors in the back, and four side (shoulder) muscles. The side muscles are alternating or directed. McCollum and Boyle [29] discuss the innervation patterns between canal neurons and muscle motoneurons—how the six canal neurons connect to the eight muscle motoneurons, and whether the connection occurs via an excitatory synapse or an inhibitory one. The pattern of connections to each muscle is given in Figure 16. It is important to understand that in Figure 16 an asterisk represents a list of the connections from canals to muscle groups, and type of signal that is transmitted along each connection.

Left Flexor (LF=3) Right Flexor (RF=6)

Left Alternating (LA=1) Left Directed (LD=7) Right Directed (RD=8) Right Alternating (RA=2)

Left Extensor (LE=5) Right Extensor (RE=4)

Figure 15: Location and numbering of eight muscle groups.

Observe that the muscle groups also partition into four polarity pairs:

$$\{LA, RA\} \quad \{LF, RE\} \quad \{LE, RF\} \quad \{LD, RD\}.$$

If one muscle in a polarity pair can and does receive an excitatory signal from a canal, then the other muscle in that polarity pair can and will receive an inhibitory signal from that canal.

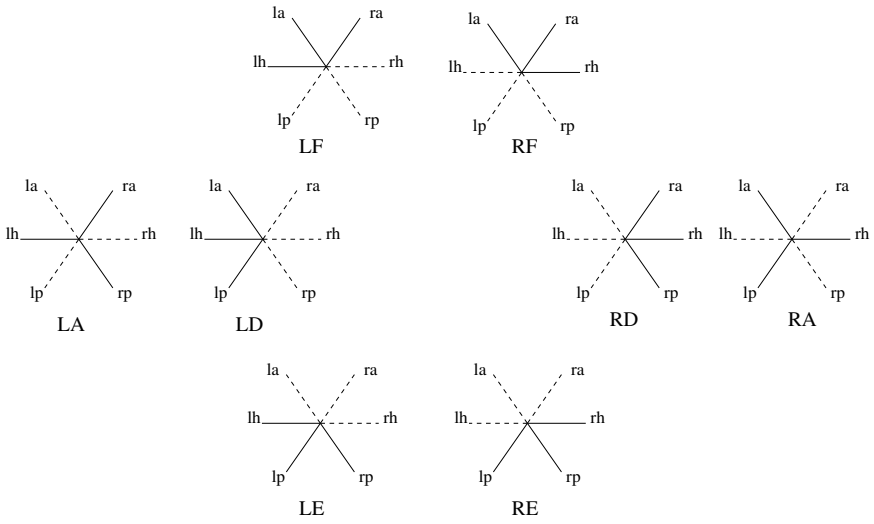

Figure 16: Innervation patterns corresponding to eight muscle groups.

We illustrate the same information in another way. McCollum and Boyle [29] consider only the *disynaptic pathway* from the six vestibular nerve afferents ('canal nerves') to the eight neck motoneurons (by way of the corresponding vestibulospinal neurons). They remark that almost always 'the motoneurons of each tested muscle responded to stimulation of all six canal nerves'. The responses were classified as either excitatory or inhibitory, as indicated by solid or dotted lines for the relevant arm of the asterisk. This description makes it clear that their Figure 4 is a diagram determining these *connections*.

Octahedral symmetry of canals and muscles

McCollum and Boyle [29] show that the symmetry group of the canal-neck projection is the octahedral group $\mathbb{O}$. We employ a geometric image in which the canals are identified with the six faces of a cube, and the muscles with the eight vertices. The group $\mathbb{O}$ acts on this picture by rigid motions of the cube in $\mathbf{R}^3$. The canals are identified with faces so that the canal polarity pairs are identified with pairs of opposite faces. Up to symmetry there is precisely one way to make this identification. Each vertex of the cube is in the intersection of exactly three faces. We identify a vertex with the asterisk whose excitatory signals correspond to the three adjoining faces. For example the unique vertex in the intersection of the three left canals (see Figure 17) is identified with the left direct muscle LD in Figure 16, since that muscle responds to excitatory signals from the three left canals.

Figure 17 can also be used to construct a schematic for the connections from canals to muscle groups. Each face of the cube (a canal) is connected to the four muscle groups corresponding to a vertex on that face by a connection that innervates that muscle group when an excitatory signal is sent from the canal. The four muscle groups corresponding to vertices on the opposite face are innervated by inhibitory signals sent from that canal. It

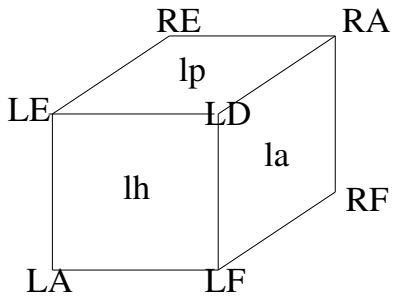

Figure 17: Identification of polarity pairs and muscle groups to the cube.

follows that any symmetry of the cube permutes canals with canals and muscle groups with muscle groups in such a way that it preserves connections and their types. Thus, in this sense, the octahedral group is the group of symmetries of the canal-neck projection.

A Minimal Phase Space for Dynamics

As we saw with the examples of gaits and the visual cortex, any mathematical analysis based on symmetry can proceed only after the symmetry group and its action on phase space have been identified. The McCollum-Boyle construction determines the symmetry group of the canal-neck projection. As discussed in [22] there is a guess as to the simplest reasonable phase space for the dynamics of this projection and hence for the representation of $\mathbb{O}$ on that phase space.

The simplest possible phase space is 14-dimensional consisting of one dimension for each canal and one dimension for each muscle group. However, the states of the canal-neck system lie in a subspace of $\mathbf{R}^{14} = \mathbf{R}^6 \times \mathbf{R}^8$. In particular, it is reasonable to identify the ith canal variable ω_i with the angular acceleration measured by that canal. Suppose that the first and second canals form a polarity pair. Since polarity pairs of canals measure opposite accelerations, we have that $\omega_2 = -\omega_1$. Similarly, it is reasonable (because of symmetry) that states of polarity pairs of muscle groups have values that are the negative of each other. Thus, the minimal state space of the canal-neck projection is $\mathbf{R}^3 \times \mathbf{R}^4 \equiv \mathbf{R}^7$.

The octahedral group has the form $\mathbb{O} = \mathbf{S}_4 \oplus \mathbf{Z}_2(-I)$, where the permutation group $\mathbf{S}_4$ corresponds to the rotational symmetries of the cube. Our discussion suggests that $-I$ permutes polarity pairs of canals and muscles and multiplies the result by -1. Thus the fixed-point subspace $\mathrm{Fix}(-I)$ of the action of $-I$ on $\mathbf{R}^{14}$ is the 7-dimensional state space we have just described. Since $\mathbf{S}_4$ commutes with $-I$, $\mathbf{S}_4$ acts on $\mathrm{Fix}(-I)$. It is a curious fact that the only nontrivial irreducible representation of $\mathbf{S}_4$ acting on the polarity pairs of muscle groups is the standard action of the rotation group of the cube acting on $\mathbf{R}^3$.

The Physiological Role of the Muscle Groups

Finally, for purposes of interpretation, we adopt a caricature of the anatomy of the muscle groups, illustrated in Figure 18. Here we assume that the principal effect of a muscle group

being activated is to pull the head in the indicated direction. Six muscle groups effectively form a 'hexagon' and their effect is to tilt the head in various directions. The other two, LA and RA, rotate the head about the vertical axis (as sensed by the horizontal canals lh, rh). There is some redundancy here: the hexagon includes three pairs of muscle groups but the three associated directions are linearly dependent. However, the use of six muscles makes the head position more stable, so there may be physiological reasons for this redundancy. McCollum and Boyle [29] call this hexagon the *central dial*.

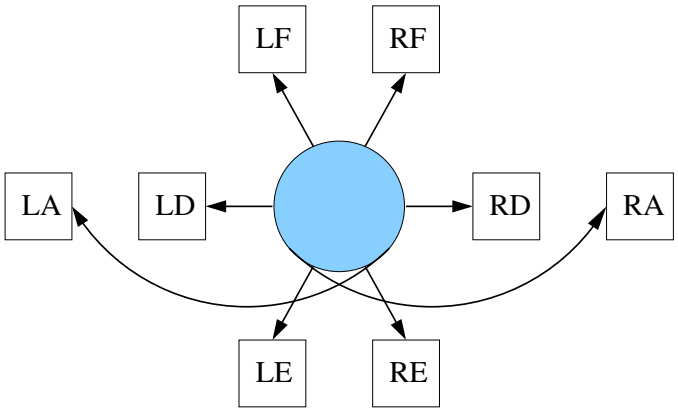

Figure 18: Caricature of effect of activation of muscle groups.

It remains to be seen whether the octahedral symmetry that is present in the canal-neck projection of the vestibular system can be used to shed light on some of the functions of that system. However, symmetry is rarely an accident.

Acknowledgments

There are many people whose ideas concerning the uses of symmetry in neuroscience were used in this report, and I would like to thank each of them: Richard Boyle, Paul Bressloff, Luciano Buono, Jim Collins, Bard Ermentrout, Gin McCollum, LieJune Shiau, Peter Thomas and Matt Wiener, and in particular, Jack Cowan and Ian Stewart. This work was supported in part by NSF Grant DMS-0244529 and in part by the Newton Institute.

References

[1] G.G. Blasdel. Orientation selectivity, preference, and continuity in monkey striate cortex, *J. Neurosci.* **12** (1992) 3139–3161.

[2] J. Blaszczyk and C. Dobrzecka. Alteration in the pattern of locomotion following a partial movement restraint in puppies. *Acta. Neuro. Exp.* **49** (1989) 39–46.

[3] W.H. Bosking, Y. Zhang, B. Schofield, and D. Fitzpatrick. Orientation selectivity and the arrangement of horizontal connections in tree shrew striate cortex, *J. Neurosci.* **17** 6 (1997) 2112–2127.

[4] P.C. Bressloff, J.D. Cowan, M. Golubitsky, and P.J. Thomas. Scalar and pseudoscalar bifurcations motivated by pattern formation on the visual cortex, *Nonlinearity* **14** (2001) 739–775.

[5] P.C. Bressloff, J.D. Cowan, M. Golubitsky, P.J. Thomas, and M.C. Wiener. Geometric visual hallucinations, Euclidean symmetry, and the functional architecture of striate cortex, *Phil. Trans. Royal Soc. London B* **356** (2001) 299–330.

[6] P.C. Bressloff, J.D. Cowan, M. Golubitsky, P.J. Thomas and M.C. Wiener. What geometric visual hallucinations tell us about the visual cortex, *Neural Computation* **14** (2002) 473–491.

[7] P.L. Buono and M. Golubitsky. Models of central pattern generators for quadruped locomotion: I. primary gaits. *J. Math. Biol.* **42** No. 4 (2001) 291–326.

[8] J. Clottes and D. Lewis-Williams. *The Shamans of Prehistory: Trance and Magic in the Painted Caves*, Abrams, New York, 1998.

[9] J.J. Collins and I. Stewart. Hexapodal gaits and coupled nonlinear oscillator models, *Biol. Cybern.* **68** (1993) 287–298.

[10] J.J. Collins and I. Stewart. Coupled nonlinear oscillators and the symmetries of animal gaits, *J. Nonlin. Sci.* **3** (1993) 349–392.

[11] J.D. Cowan. Some remarks on channel bandwidths for visual contrast detection. *Neurosciences Research Program Bull.* **15** (1977) 492–517.

[12] G.B. Ermentrout and J.D. Cowan. A mathematical theory of visual hallucinations, *Biol. Cybern.* **34** (1979) 137–150.

[13] U. Eysel. Turning a corner in vision research, *Nature* **399** (1999) 641–644.

[14] P.P. Gambaryan. *How Mammals Run: Anatomical Adaptations*, Wiley, New York 1974.

[15] C.D. Gilbert. Horizontal integration and cortical dynamics, *Neuron* **9** (1992) 1–13.

[16] M. Golubitsky, L-J. Shiau and A. Torok. Bifurcation on the visual cortex with weakly anisotropic lateral coupling. *SIAM J. Appl. Dynam. Sys.* **2** (2003) 97–143.

[17] M. Golubitsky and I. Stewart. *The Symmetry Perspective: From Equilibrium to Chaos in Phase Space and Physical Space*. Progress in Mathematics **200**, Birkhäuser, Basel, 2002.

[18] M. Golubitsky and I. Stewart. Nonlinear dynamics of networks: the groupoid formalism. *Bull. Amer. Math. Soc.*. To appear.

[19] M. Golubitsky, I. Stewart, P.-L. Buono, and J.J. Collins. A modular network for legged locomotion, *Physica D* **115** (1998) 56–72.

[20] M. Golubitsky, I. Stewart, P.-L. Buono, and J.J. Collins. Symmetry in locomotor central pattern generators and animal gaits, *Nature* **401** (1999) 693–695.

[21] M. Golubitsky, I. Stewart, and D.G. Schaeffer. *Singularities and Groups in Bifurcation Theory II*, Applied Mathematics Sciences, **69**, Springer-Verlag, New York, 1988.

[22] M. Golubitsky, I. Stewart, and L.J. Shiau. Spatio-temporal symmetries in the disynaptic canal-neck projection. In preparation.

[23] M. Golubitsky, I. Stewart, and A. Török. Patterns of synchrony in coupled cell networks with multiple arrows, *SIAM J. Appl. Dynam. Sys.* **4**(1) (2005) 78–100.

[24] S. Grillner, D. Parker, and A.J. El Manira. Vertebrate locomotion—a lamprey perspective, *Ann. New York Acad. Sci.* **860** (1998) 1–18.

[25] S. Grillner and P. Wallén. Central pattern generators for locomotion, with special reference to vertebrates, *Ann. Rev. Neurosci* **8** (1985) 233–261.

[26] D.H. Hubel and T.N. Wiesel. Sequence regularity and geometry of orientation columns in the monkey striate cortex, *J. Comp. Neurol.* **158** No. 3 (1974) 267–294; Uniformity of monkey striate cortex: a parallel relationship between field size, scatter, and magnification factor, *J. Comp. Neurol.* **158** No. 3 (1974) 295–306; Ordered arrangement of orientation columns in monkeys lacking visual experience, *J. Comp. Neurol.* **158** No. 3 (1974) 307–318.

[27] H. Klüver. *Mescal and Mechanisms of Hallucinations*. University of Chicago Press, Chicago, 1966.

[28] N. Kopell and G.B. Ermentrout. Coupled oscillators and the design of central pattern generators, *Math. Biosci.* **90** (1988) 87–109.

[29] G. McCollum and R. Boyle. Rotations in a vertebrate setting: evaluation of the symmetry group of the disynaptic canal-neck projection. *Biol. Cybern.* **90** (2004) 203–217.

[30] A. Patterson. *Rock Art Symbols of the Greater Southwest*, Johnson Books, Boulder CO, 1992, 185.

[31] E. Schwartz. Spatial mapping in the primate sensory projection: analytic structure and relevance to projection, *Biol. Cybernetics* **25** (1977) 181–194.

[32] G. Schöner, W.Y. Jiang, and J.A. Kelso. A synergetic theory of quadrupedal gaits and gait transitions, *J. Theor. Biol.* **142** No 3 (1990) 359–391.

[33] R.K. Siegel and M.E. Jarvik. Drug–induced hallucinations in animals and man. In: *Hallucinations: Behavior, Experience and Theory*, (R.K. Siegel and L.J. West, eds.) Wiley, New York, 1975, 81–161.

[34] L.C. Sincich and G.G. Blasdel. Oriented axon projections in primary visual cortex of the monkey. *J. Neurosci.* **21** (2001) 4416–4426.

[35] I. Stewart, M. Golubitsky, and M. Pivato. Patterns of synchrony in coupled cell networks. *SIAM J. Appl. Dynam. Sys* **2** (2003) 609–646. [DOI: 10.1137/S1111111103419896]

[36] T. Vilis. The physiology of the senses, Lecture 10: Balance, www.med.uwo.ca/physiology/courses/sensesweb

[37] H.R. Wilson and J.D. Cowan. Excitatory and inhibitory interactions in localized populations of model neurons, *Biophys. J.* **12** (1972) 1–24.